We compute the afterglow of gamma-ray bursts produced by purely electromagnetic outflows to see if it shows characteristic signatures differing from those obtained with the standard internal/external shock model. Using a simple approach for the injection of electromagnetic energy to the forward shock we obtain the afterglow evolution both during the period of activity of the central source and after. Our method equally applies to a variable source. Afterglow light curves in the visible and X-ray bands are computed both for a uniform medium and a stellar wind environment. They are brighter at early times than afterglows obtained with the internal/external shock model but relying only on these differences to discriminate between models is not sufficient.

Key words. Gamma rays: bursts; Radiation mechanisms: non-thermal

arXiv:astro-ph/0607565v1 25 Jul 2006

Astronomy & Astrophysics manuscript no. blm
(DOI: will be inserted by hand later)

Afterglow calculation in the electromagnetic model for gamma-ray bursts

F. Genet, F. Daigne & R. Mochkovitch

Institut d'Astrophysique de Paris - UMR 7095 CNRS et Université Pierre et Marie Curie,
98 bis, boulevard Arago, 75014 Paris, France
e-mail: genet@iap.fr

the date of receipt and acceptance should be inserted later

Abstract.

1. Introduction

Lyutikov and Blandford (2003) proposed an alternative to the standard fireball model where the central engine produces a purely electromagnetic outflow instead of a relativistic baryonic wind. Observationally this electromagnetic model (hereafter EMM) differs from the standard internal/external shock model by the absence of any reverse shock contribution, a different early afterglow evolution and a high polarization of the prompt emission (Lyutikov, 2004). In this paper we concentrate on the early afterglow (while the central source is still active) and compare the EMM to the standard model in X-rays and the visible for a uniform external medium or a wind environment. In Sect.2 we obtain simple equations that govern the evolution of the forward shock propagating in the burst environment. Their solutions are used in Sect.3 to compute afterglow light curves which are compared to those obtained in the standard model for the same total injected energy. We discuss our results in Sect.4 and conclude that it likely will be difficult to decide between models from afterglow observations only.

2. Dynamics of the forward shock

In the context of the EMM, electromagnetic energy released by the central source directly leads to the formation of a forward shock propagating in the external medium. We obtain the evolution of this forward shock by writing the conservation of energy-momentum of the swept-up mass as it accumulates electromagnetic energy

$$\begin{aligned} E_{\rm EM} + Mc^2 &= M\Gamma\Gamma_i c^2 \\ E_{\rm EM} &= M\beta\Gamma\Gamma_i c^2 \end{aligned} \tag{1}$$

where M is the swept-up mass, β and Γ the velocity and Lorentz factor for the bulk motion of the shocked material and Γ_i the Lorentz factor for internal motions. The energy $E_{\rm EM}$ received from the source reads

$$E_{\rm EM} = \int_0^{t_s} L_{\rm EM}(t)dt \tag{2}$$

where $L_{\rm EM}(t)$ is the source electromagnetic power and t_s the time in the source frame (which is also the observer time modulo the $(1+z)$ factor for time dilation).

This can be easily understood if we define the time t_e when the shocked material is located at radius R. The emitted afterglow signal will reach the observer at

$$t_{\rm obs} = t_e + \frac{(D-R)}{c} \tag{3}$$

where D is the distance of the source to the observer. At time t_e, all power produced by the source up to a time t_s such as

$$c(t_e - t_s) = R \tag{4}$$

has been received by the moving shell and Eq.(3) and (4) then lead to

$$t_{\rm obs} = t_s + \frac{D}{c}\,. \tag{5}$$

Going back to Eq.(1) and after elimination of Γ_i we get

$$2Mc^2\Gamma^2 \sim E_{\rm EM} \tag{6}$$

this approximation being valid in the relativistic phase ($\Gamma \gg 1$). Differentiation of Eq.(6) with respect to observer time (with the simplified notation $t = t_{\rm obs}$) yields

$$L_{\rm EM}(t) = \frac{16\pi A c^2}{3-s}\left(R^{3-s}\,\Gamma\frac{d\Gamma}{dt} + (3-s)\,cR^{2-s}\Gamma^4\right) \tag{7}$$

where we have written

$$M(R) = \frac{4\pi A}{3-s}R^{3-s} \tag{8}$$

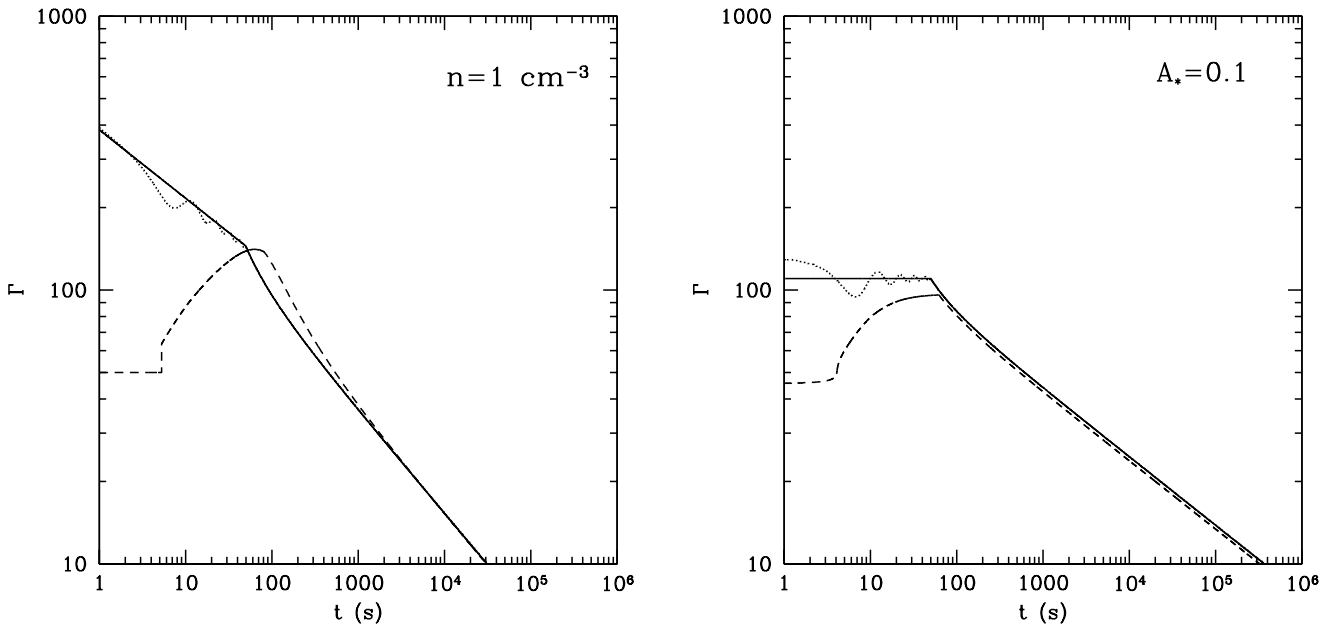

Fig. 1. Evolution of the Lorentz factor in the different models considered; left panel: uniform external medium of density $n = 1$ cm^{-3}; right panel: stellar wind with $A_* = A/(5\,10^{11}$ g.cm$^{-1}) = 0.1$. The full, dotted and dashed lines respectively correspond to the EMM with a constant $L_{\rm EM} = 10^{52}$ erg.s^{-1}, a variable $L_{\rm EM}(t)$ given by Eq.(13) and to the standard internal/external shock model with $\dot{E} = 10^{52}$ erg.s^{-1} and an initial distribution of the Lorentz factor in the relativistic wind given by Eq.(14).

with $A = \rho$ and $s = 0$ for a uniform medium of density ρ and $A = 5\,10^{11} A_*$ g.cm^{-1} and $s = 2$ for a wind environment. With the additional relation between observer time and shock radius

$$\frac{dR}{dt} = 2c\Gamma^2 \tag{9}$$

the problem can be solved for any law $L_{\rm EM}(t)$. With a constant $L_{\rm EM}$ it can be easily shown that the solutions of Eq.(7) and (9) are

$$\Gamma = (Q/2)^{1/2}\,(ct)^{-1/4} \quad \text{and} \quad R = 2Q(ct)^{1/2} \tag{10}$$

with

$$Q = \left(\frac{3L_{\rm EM}}{32\pi\rho c^3}\right)^{1/4} \tag{11}$$

for a uniform medium and

$$\Gamma = \left(\frac{L_{\rm EM}}{16\pi A c^3}\right)^{1/4} \quad \text{and} \quad R = 2c\Gamma^2 t \tag{12}$$

for a stellar wind. With a variable $L_{\rm EM}(t)$, Eq.(7) and (9) are integrated using Eq.(10) or (12) as initial conditions with $L_{\rm EM} = L_{\rm EM}(t = 0)$. Figure 1 shows the resulting $\Gamma(t)$ for a constant $L_{\rm EM} = 10^{52}$ erg.s^{-1} or $L_{\rm EM}(t)$ given by

$$L_{\rm EM}(t) = 10^{52}\left[1 + \cos 2\pi\left(\frac{t}{10\,\rm s}\right)\right] \quad \text{erg.s}^{-1}\ . \tag{13}$$

In both cases the source is supposed to be active for 50 s. For comparison we also plot in Fig.1 the evolution of the Lorentz factor computed in the standard internal/external shock model. In that case, we assume that a constant kinetic power $\dot{E} = 10^{52}$ erg.s^{-1} is injected in the relativistic wind for a duration $t_{\rm W} = 50$ s. We consider a single pulse burst produced by a distribution of the Lorentz factor of the form

$$\Gamma(t) = \frac{\Gamma_{\rm max} + \Gamma_{\rm min}}{2} - \frac{\Gamma_{\rm max} - \Gamma_{\rm min}}{2}\cos\left(\pi\frac{t}{0.2\,t_{\rm W}}\right) \tag{14}$$

if $t < 0.2\,t_{\rm W}$ and $\Gamma(t) = \Gamma_{\rm max}$ if $t > 0.2\,t_{\rm W}$; $\Gamma_{\rm max} = 200$ and $\Gamma_{\rm min} = 50$ are the maximum and minimum values of the Lorentz factor so that the most rapid part of the wind is decelerated by the slower one which was emitted previously. To follow the wind evolution and its interaction with the external medium we represent the flow with a large number ($\gtrsim 1000$) of discrete shells which interact by direct collision only, pressure waves being neglected (Daigne and Mochkovitch, 1998). The action of the external medium is included by progressively adding the swept-up mass to the front shell of the wind. In all cases, the Lorentz factor relaxes to the standard Blandford-McKee (1976) solution after a few 10^2 s. However at early times Γ is larger in the EMM, especially for a uniform external medium.

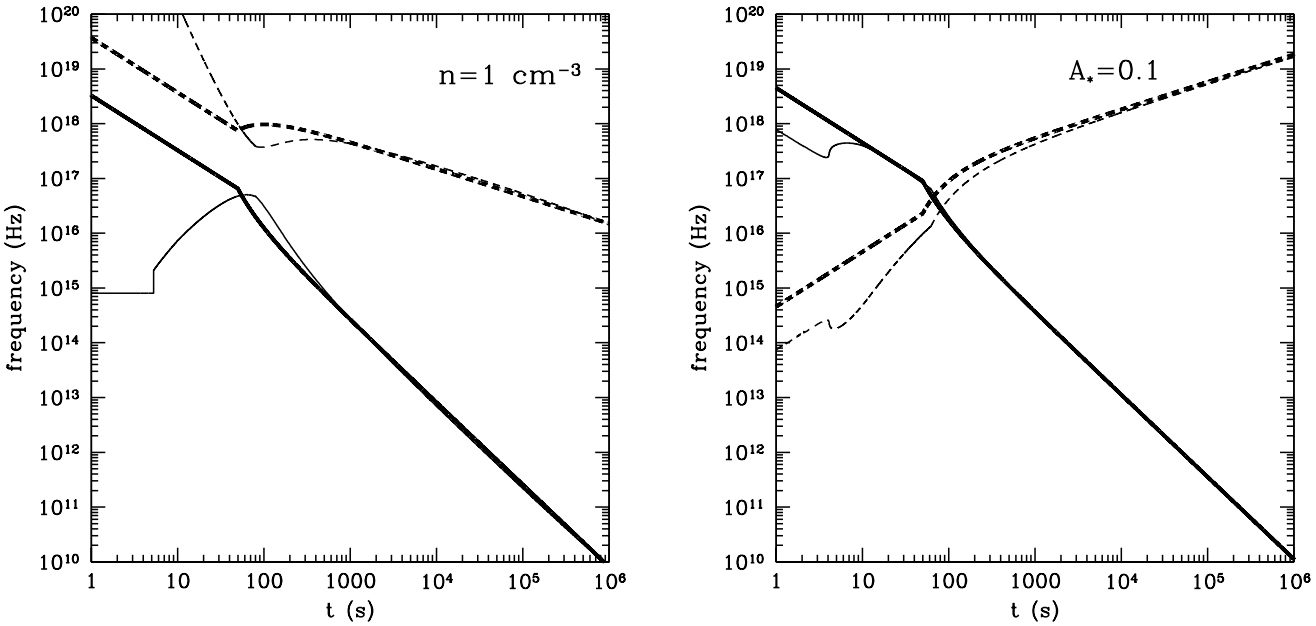

Fig. 2. The two frequencies ν_m (full lines) and ν_c (dashed lines) in the EMM (thick lines) and the standard model (thin lines); left panel: uniform external medium of density $n = 1$ cm^{-3}; right panel: stellar wind with $A_* = 0.1$.

3. Afterglow calculation

3.1. Method

Using the dynamical evolution of the forward shock obtained above we have calculated afterglow lightcurves in X-rays and in the V band for both the electromagnetic and the standard model. We obtain the two critical frequencies ν_m and ν_c following Sari, Piran and Narayan (1998). They are represented in Fig.2 for a uniform medium and a stellar wind environment. In the EMM with a uniform medium and a constant source, the ratio ν_m/ν_c is given by

$$\frac{\nu_m}{\nu_c} = 0.065\,\epsilon_{e,-1}^2\epsilon_{B,-3}^2\,n\,L_{52} \qquad (15)$$

where n is the density in cm^{-3}, L_{52} the electromagnetic power in units of 10^{52} erg.s^{-1}, $\epsilon_{e,-1} = \epsilon_e/10^{-1}$ and $\epsilon_{B,-3} = \epsilon_B/10^{-3}$ (the numerical factor in Eq.(15) corresponding to the electron power law index $p = 2.5$). The cooling regime therefore remains fixed as long as the source is active (and does not vary). In Fig.2 we have adopted $\epsilon_{e,-1} = \epsilon_{B,-3} = L_{52} = 1$ and $n = 1$ or $A_* = 0.1$ in the uniform medium or wind case respectively.

With these parameters the afterglow is always in the slow cooling regime in the uniform medium case while in the wind case it is in fast cooling while the source is active and moves to slow cooling shortly after.

3.2. Results

We have represented in Fig.3 afterglow light curves in X-rays (2 - 10 keV) and in the V band for a uniform external medium and a stellar wind. The burst parameters are identical to those used in Fig.2. For comparison we also show in Fig.3 standard afterglows computed in the internal/external shock model with the same total injected energy. A redshift $z = 2$, typical of SWIFT bursts has been adopted (Jakobsson et al., 2006). In all cases the afterglows are brighter at early times in the EMM while at late times (in the Blandford-McKee regime) the models coincide. The difference in early evolution is larger for a uniform external medium, especially in X-rays. This is due to the large initial Lorentz factor in the EMM compared to the standard model (see Fig.1) which leads to a higher electron Lorentz factor in the shocked external medium. The frequency ν_m is then in the X-ray band already at very early times while it is still in the UV/visible in the standard model. In the wind case, the differences between the EMM and the standard case are smaller and the two models will be therefore more difficult to distinguish.

For the EMM we have also calculated afterglows when the source is variable (with $L_{\rm EM}(t)$ given by Eq.(13)). The results are shown in Fig.4 for a uniform external medium and the first 200 seconds of evolution (the source being active for 150 s in the observer frame). The left panel in Fig.4 shows the simple calculation which only includes line of sight emission. It produces a highly variable X-ray light curve but off-axis effects (time delays and spectral softening) will smear out any variability occurring on a time scale shorter than

$$\Delta t = \frac{R}{2c\Gamma^2} \qquad (16)$$

where R and Γ are the radius and Lorentz factor of the emitting shell. The right panel of Fig.4 shows Δt as a func-

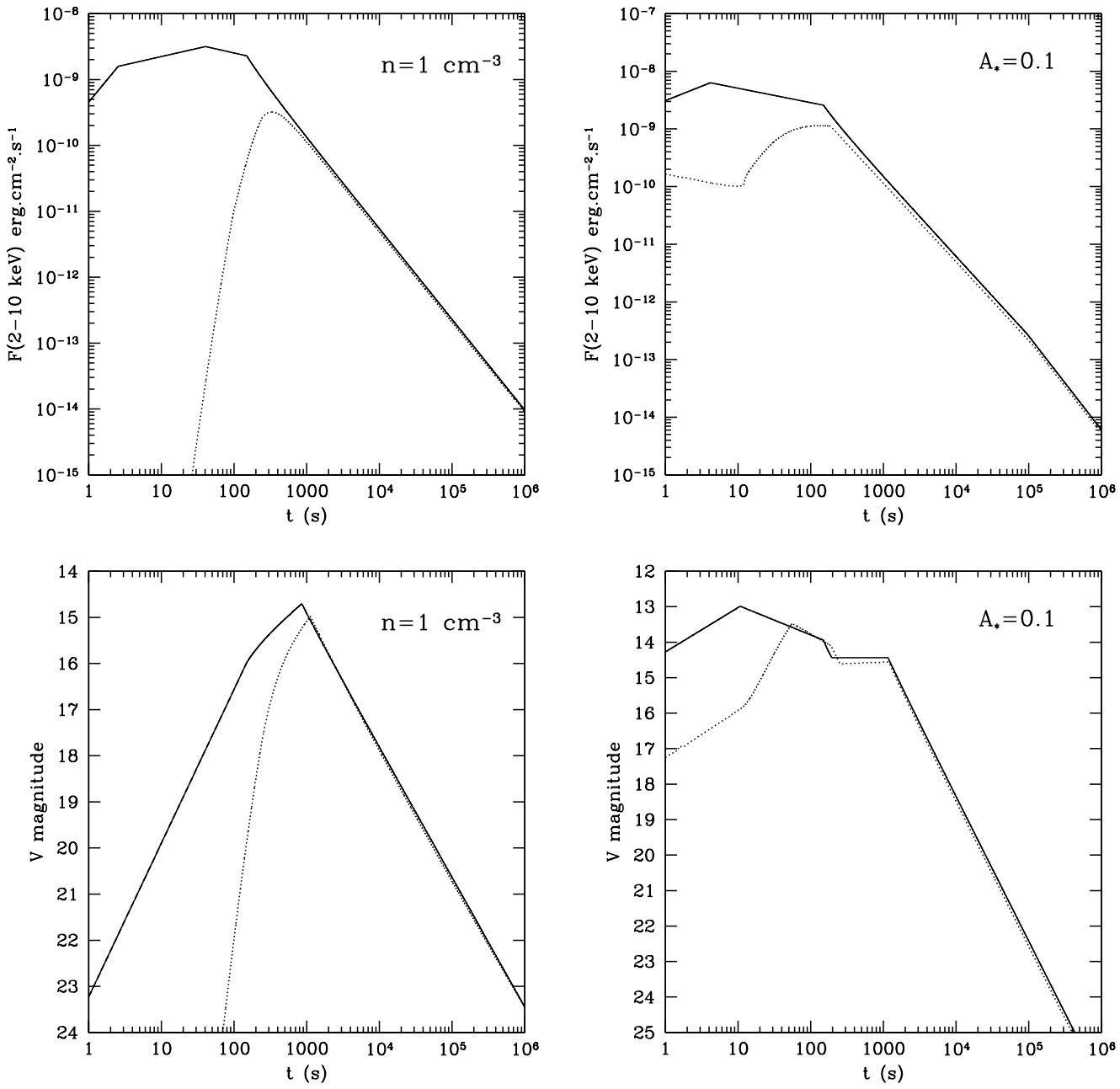

Fig. 3. Afterglow comparison between the EMM (solid line) and the standard model (dotted line). Top: X-ray band (2 - 10 keV); Bottom: V band; Left column: uniform medium of density $n = 1$ cm^{-3}; right column: stellar wind with $A_* = 0.1$. A redshift $z = 2$ has been assumed.

tion of observer time together with the X-ray light curve now obtained with a detailed calculation including off-axis effects (Granot, Piran & Sari, 1999; Woods & Loeb, 1999). Except for the first two or three peaks which partially subsist because Δt is initially small, the rest of the curve becomes nearly monotonic. In the visible the variability is barely visible, even without including off-axis effects.

4. Discussion and conclusion

The lightcurves in Fig.3 show that the EMM and the standard model notably differ at early times (during the period of source activity). However relying on these differences alone to identify the physical origin of GRBs will be a difficult task requiring a very early follow-up of the afterglow. In X-rays, SWIFT should be able to do that (at least in some cases) but the problem here will come from the mixing of the afterglow contribution with the brighter prompt emission component. This mixing will also probably pre-

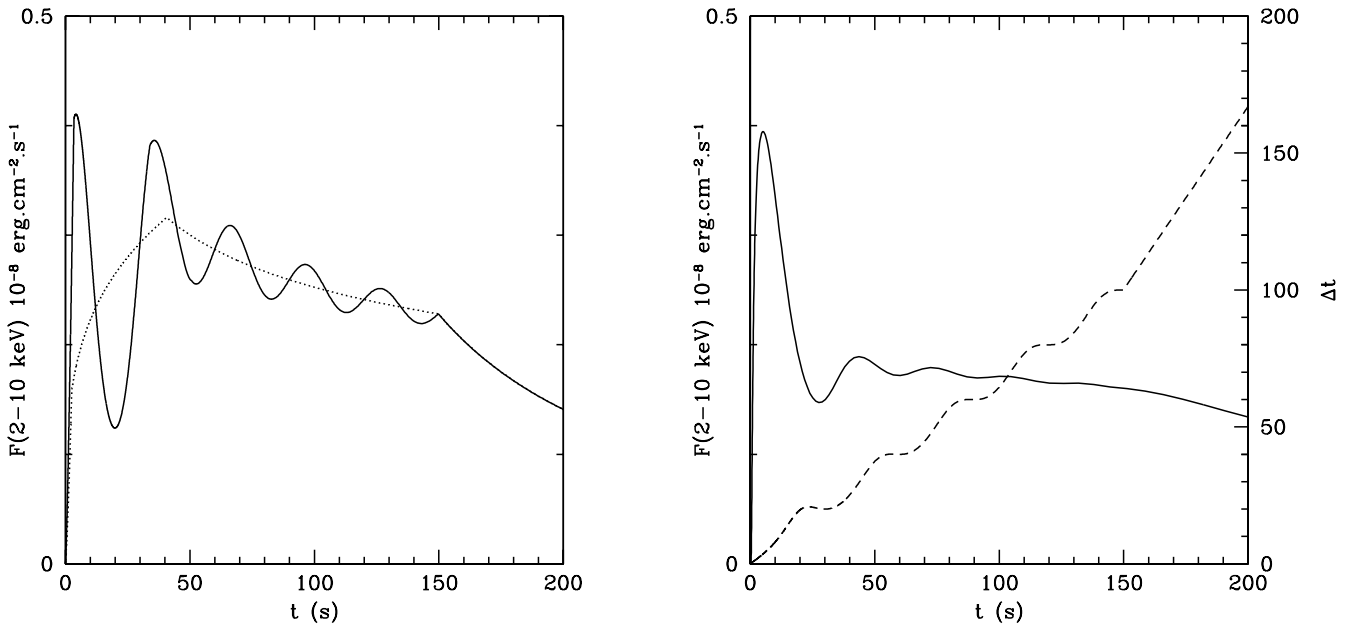

Fig. 4. Early afterglows for a variable source ($L_{\rm EM}(t)$ being given by Eq.(13)). Left panel: afterglow computed with on-axis emission only compared to the case of a constant source (dotted line). Right panel: afterglow computed with off-axis emission included (full line) and geometrical delay $\Delta t = R/2c\Gamma^2$ (dashed line). A uniform external medium of density $n = 1$ cm^{-3} and a redshift $z = 2$ have been assumed.

vent an unambiguous detection of the imprint of source variability on the X-ray afterglow (Fig.4). In the visible, where the burst prompt emission is weak and probably negligible (see however the recent RAPTOR observations of GRB 041219a and GRB 050820a (Vestrand et al., 2005, 2006)), the EMM predicts a brighter afterglow for a given set of parameters ϵ_e, ϵ_B, n or A_*. But in real afterglows these parameters are not known a priori and deciding between models will be tricky. Polarization properties of the burst prompt emission (Lyutikov, 2004) when they become more easily accessible may provide clearer evidence.

A last interesting point concerning the EMM is related to the shallow part observed by SWIFT in many X-ray afterglows. The light curves in Fig. 3 show that the EMM indeed predicts an initially flat region in the early X-ray afterglow. However this flat region does not last more than the period of source activity (150 s in observer time in Fig.3). It would then extend to 10^4 s (or more) only if the source can remain active for that duration, as was also suggested for the standard model (Zhang et al., 2005).

References

Blandford, R.D. & McKee, C.F. 1976, PhFl 19, 1130.
Daigne, F., & Mochkovitch, R. 1998, MNRAS, 296, 275.
Granot, J., Piran, T. & Sari, R. 1999, ApJ, 513, 679.
Jakobsson, P., Levan, A., Fynbo, J.P.U. et al., 2006, A&A 447, 897.
Lyutikov, M. & Blandford, R.D., 2003, astro-ph/0312347.
Lyutikov, M., 2004, 35th COSPAR Meeting, astro-ph/0409489.
Sari, R., Piran, T. & Narayan, R., 1998, ApJ 497, L17.
Vestrand, W.T., Wozniak, P.R., Wren, J.A. et al., 2005, Nature 435, 178.
Vestrand, W.T., Wren, J.A., Wozniak, P.R. et al., 2006, to appear in Nature.
Woods, E., & Loeb, A. 1999, ApJ, 523, 187.
Zhang, B., Fan, Y.Z., Dyks, J. et al. 2006, ApJ 642, 354.